Molecular Therapy
Oncolytics
Original Article

Intravesical immunotherapy with a GM-CSF armed oncolytic vesicular stomatitis virus improves outcome in bladder cancer

Coby Rangsitratkul,[1,8] Christine Lawson,[1,8] Francis Bernier-Godon,[1] Seyedeh-Raheleh Niavarani,[1] Marie Boudaud,[2] Samuel Rouleau,[1] Antoine-Olivier Gladu-Corbin,[3] Abera Surendran,[4] Nadia Ekindi-Ndongo,[5] Madhuri Koti,[6] Carolina S. Ilkow,[4] Patrick O. Richard,[3,7] and Lee-Hwa Tai[1,7]

[1]Department of Immunology and Cell Biology, Université de Sherbrooke, Sherbrooke, QC J1E 4K8P, Canada; [2]Department of Pediatrics, Université de Sherbrooke, Sherbrooke, QC J1H 5N4, Canada; [3]Department of Surgery, Division of Urology, Université de Sherbrooke, Sherbrooke, QC J1H 5N4, Canada; [4]Centre for Innovative Cancer Therapeutics, Ottawa Hospital Research Institute, Ottawa, ON K1H 8L6P, Canada; [5]Department of Pathology, Université de Sherbrooke, Sherbrooke, QC J1H 5N4P, Canada; [6]Department of Biomedical and Molecular Sciences, Queen's University, Kingston, ON K7L 3N6, Canada; [7]Centre de Recherche du CHUS, Sherbrooke, QC J1H 5N4, Canada

A significant proportion of non-muscle invasive bladder cancer cases will progress to muscle invasive disease. Transurethral resection followed by Bacillus Calmette Guerin immunotherapy can reduce this risk, while cystectomy prior to muscle invasion provides the best option for survival. Currently, there are no effective treatments for Bacillus Calmette Guerin refractory disease. A novel oncolytic vesicular stomatitis virus containing the human GM-CSF transgene (VSVd51-hGM-CSF) was rescued and tested as a potential bladder-sparing therapy for aggressive bladder cancer. The existing variant expressing mouse GM-CSF was also used. Measurement of gene expression and protein level alterations of canonical immunogenic cell death associated events on mouse and human bladder cancer cell lines and spheroids showed enhanced release of danger signals and immunogenic factors following infection with VSVd51-m/hGM-CSF. Intravesical instillation of VSVd51-mGM-CSF into MB49 bladder cancer bearing C57Bl/6 mice demonstrated enhanced activation of peripheral and bladder infiltrating effector immune cells, along with improved survival and reduced tumor volume. Importantly, virus-mediated anti-tumor immunity was recapitulated in bladder cancer patient-derived organoids. These results suggest that VSVd51-hGM-CSF is a promising viro/immunotherapy that could benefit bladder cancer patients.

INTRODUCTION

Bladder cancer (BC) is the fourth most common cancer for men[1,2] and is the most expensive solid cancer to treat due to the requirement for specialized monitoring equipment and highly trained personnel.[3,4] At initial diagnosis, approximately 75% of the cases are non-muscle-invasive bladder cancer (NMIBC) with a significant proportion that will progress to muscle-invasive disease.[2] Transurethral resection (TUR) followed by intravesical chemotherapy or Bacillus Calmette Guerin (BCG) immunotherapy can reduce this risk,[1,5,6] while cystectomy prior to muscle invasion provides the best option for survival.[7,8] However up to 84% of patients are unable to complete the 3-year BCG regimen due to local or systemic toxicity and experience BCG refractory disease.[9] There are currently no effective treatments for patients who fail BCG and are ineligible or refuse cystectomy.

Recent studies have shown that BCG and interferon (IFNα) combination therapy may be useful as salvage regimen in BCG failures.[9,10] However, various tumors acquire defects in their ability to respond to IFNs as they evolve, and many aggressive BC cell lines are highly resistant to IFN treatment.[10] IFN-resistance confers a growth advantage for cancer cells over normal tissues, but simultaneously compromises their antiviral response. To exploit this vulnerability, Zhang et al. used oncolytic vesicular stomatitis virus (VSV) that possesses the ability to selectively replicate in and kill IFN-resistant BC cells, but is strongly suppressed in IFN-responsive normal tissues.[11,12] The tumor specificity of wild-type VSV has been further enhanced in an attenuated strain (VSVd51) with a point mutation in the matrix protein, which has a defect in its ability to inhibit production and antiviral activities of IFNs. This provides enhanced protection in normal tissues, while maintaining oncolytic ability.[13] Importantly, the lack of pre-existing neutralizing antibodies in human populations, a major hurdle that impedes the *in vivo* delivery of many other oncolytic viruses (OV), warrants the development of oncolytic VSV for clinical applications.[14,15] *In vivo* experiments using IFN-resistant BC cell lines implanted in athymic nude mice demonstrated significantly reduced tumor growth following intravesical instillation with VSVd51.[12]

Received 20 July 2021; accepted 27 January 2022;
https://doi.org/10.1016/j.omto.2022.01.009.

[8]These authors contributed equally

Correspondence: Lee-Hwa Tai, Université de Sherbrooke, 3201 rue Jean-Mignault, Sherbrooke, QC J1E 4K8, Canada.
E-mail: lee-hwa.tai@usherbrooke.ca

Despite these promising preclinical results, the absence of the immune microenvironment is a significant limitation of these xenograft models. There is strong evidence to suggest that the immune system plays a critical role in determining the outcome of oncolytic VSV therapy.[16] We and others have shown that manipulating host immunity can both improve and impede the success of virotherapy.[16–18] It is not known how the presence of a functional immune system affects the response to OV treatment in mouse models of BC and its efficacy in human BC patients.

VSV-based virotherapy is in several phase I trials for solid tumors. Administration of VSV-hIFNβ-NIS monotherapy and in combination with avelumab (NCT02923466) or pembrolizumab (NCT03647163) is currently underway in patients with refractory solid tumors to determine the safety, maximum tolerated dose, pharmacokinetics, and tumor biomarkers. For late-stage melanoma patients, a phase III/IV study using VSV-hIFNβ-TYRP1 is currently testing both intravenous and intratumoral administration (NCT03865212). In BC, many different OVs have been examined in preclinical and early phase clinical studies for their oncolytic properties. Annels et al. demonstrated the immunogenic potential of coxsackie virus CVA21 by measuring immunogenic cell death (ICD) biomarkers following infection in cell lines and tissue slices, but immune functional assays were not conducted.[19] Ramesh et al. reported preclinical BC results using oncolytic adenovirus (CG0070), which encodes human granulocyte macrophage colony stimulating factor (GM-CSF). GM-CSF, an important myelopoietic growth factor, has attracted great interest as an immune stimulatory transgene to boost the therapeutic efficacy of OVs.[20–22] GM-CSF exerts its antitumor activity through enhancing conventional dendritic cell (cDC) activation and antigen presentation, in addition to improving T cell functions indirectly, in an interleukin 1 (IL1)–dependent manner.[23] While CG0070 showed significant tumor killing in xenograft mouse models, the human GM-CSF encoded by this adenovirus is species specific. Therefore, the antitumor effects observed in mice were solely attributed to the oncolytic activity of the virus.[22] Most recently, in a phase 3 study, a replication-deficient adenovirus that delivers human IFNα-2b into the bladder epithelium was tested in BCG-unresponsive NMIBC patients. In early reports, approximately, 53% of 103 patients with carcinoma *in situ* had a complete response within 3 months of the first dose, and half of these patients maintained their response at 12 months. Similar to previous studies, the underlying immune response was not evaluated.[24] Although the viral candidates described above have shown promising preclinical and early clinical results, the antitumor immune response has not been sufficiently characterized in either immunocompetent mouse models or human studies. Therefore, there is uncertainty in the ability of OV to provoke an antitumor immune response and have improved efficacy over frontline therapies for BC.

We, therefore, engineered a VSVd51 variant containing human GM-CSF (VSVd51-hGM-CSF) that has not been previously reported. Of note, several VSVd51 variants containing mouse GM-CSF have been previously described in preclinical models of melanoma and breast tumors where immune-activating properties of the recombinant virus accentuated viral oncolysis.[25,26] Using both the human and the existing mouse variant (VSVd51-mGM-CSF, Auer group), we evaluated their ability to treat BC. BC cell lines were assessed for susceptibility to viral lysis and expression of ICD markers and immune gene signatures. We hypothesized that VSVd51 containing mouse or human GM-CSF could enhance ICD signatures in mouse or human BC cells, respectively. Furthermore, we investigated the immunogenicity and therapeutic efficacy of VSVd51-mGMCSF in the C57Bl/6-MB49 syngeneic model to understand the underlying *in vivo* immune contributions of this OV. Using human BC patient-derived organoids, we measured the immune-stimulating effects of VSVd51-hGM-CSF on autologous patient immune cells to establish greater predictive power of this novel virotherapy.

RESULTS

Characterization of a VSVd51 oncolytic virus encoding human GM-CSF

Due to the therapeutic potential of GM-CSF, a human GM-CSF transgene was incorporated into the backbone of the oncolytic VSVd51 variant to create VSVd51-hGM-CSF (Figure 1A). This replication-competent OV could infect human BC cell lines with an efficiency comparable to parental VSVd51, and expression of hGM-CSF did not negatively affect viral replication (Figures 1B and 1C). Human GM-CSF was quantified in the culture media of 5637 and UM-UC-3 cell lines infected with VSVd51-hGM-CSF (Figure 1D). The mouse variant, VSVd51-mGM-CSF, was also able to infect and replicate in a mouse MB49 BC cell line (Figures S1A–S1C). Therefore, VSVd51-hGM-CSF could successfully infect human BC cells, the virus could replicate, and GM-CSF was secreted, resulting in a functional VSVd51-hGM-CSF.

The GM-CSF transgene in VSVd51 induces enhanced immunogenic cell death and associated gene signature in the MB49 mouse bladder cancer cell line following infection

There is strong evidence to suggest that the immune system plays a critical role in determining the outcome of VSV therapy. We first characterized the immunogenic potential of VSVd51 and VSVd51-mGM-CSF to treat BC. Given the importance of the mode of tumor cell death in initiating anti-tumor immune responses,[27,28] we assessed ICD following infection of the mouse MB49 cell line with VSVd51 or VSVd51-mGM-CSF. We measured high-mobility group box 1 (HMGB1) protein (Figure 2A) and adenosine triphosphate (ATP) (Figure 2B) in the supernatant of infected cells at various time points post-infection. Both HMGB1 and ATP are important biomarkers of ICD. We observed increased ATP release following 24 h of infection and similar HMGB1 levels by the VSVd51-mGM-CSF compared with controls. Another feature of necrosis is the presence of cell surface externalized calreticulin. Following virus infection, we observed an increase in the percentage of calreticulin^{+} cells in VSVd51-mGM-CSF-treated cells at 48 h post-infection (Figure 2C). Together, the presence of these heightened danger-associated molecular patterns (DAMPs) suggest a greater induction of ICD by VSVd51-mGM-CSF.

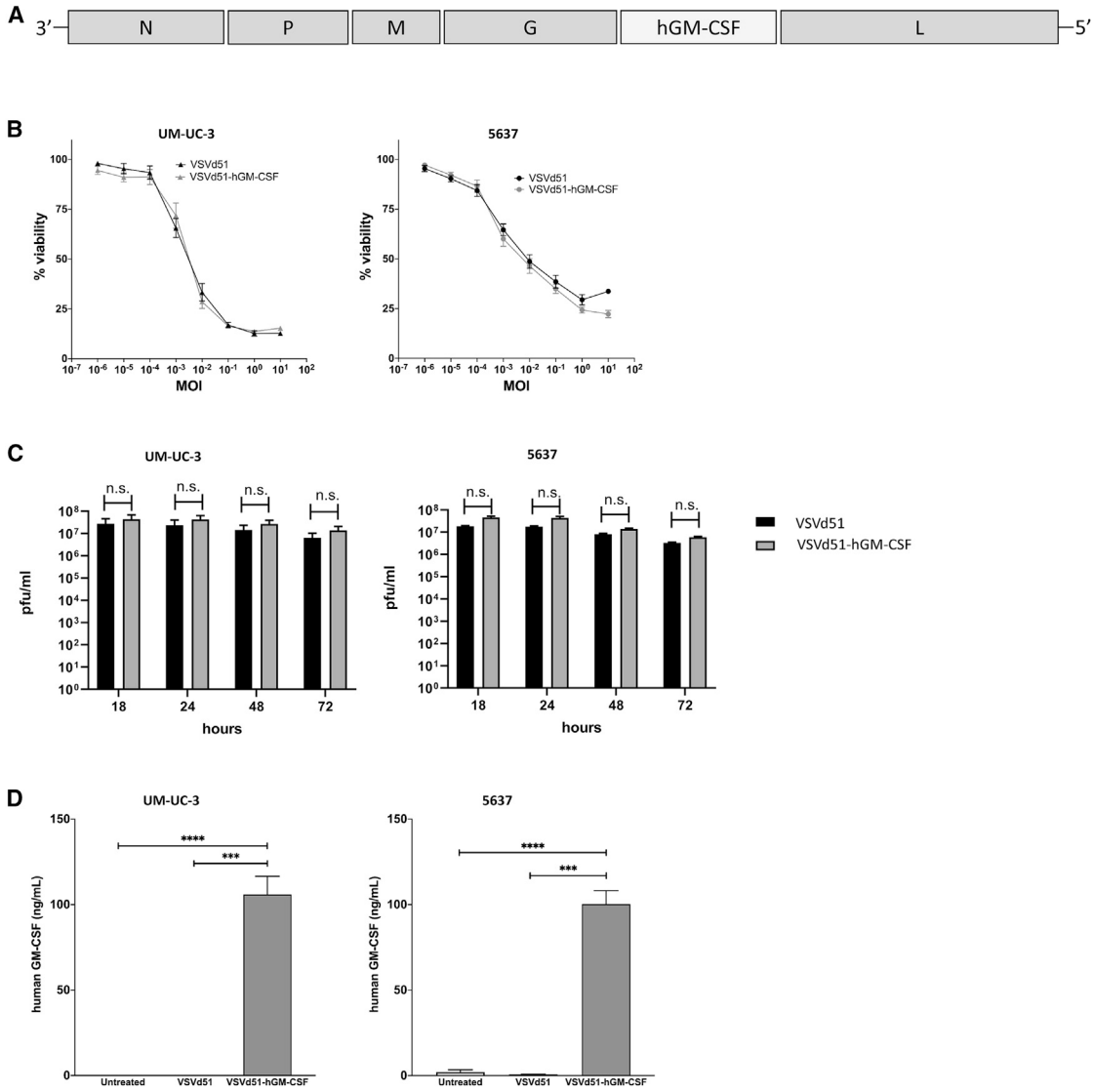

Figure 1. Characterization of a VSVd51 oncolytic virus encoding human GM-CSF

(A) A schematic of the VSVd51-hGM-CSF genome. (B) Cytotoxicity of VSVd51 and VSVd51-hGM-CSF was assessed in UM-UC-3 and 5637 BC cells at the indicated MOIs 48 h after infection. (C) Viral titers produced from VSVd51- and VSVd51-hGM-CSF-infected BC cells. (D) The amount of hGM-CSF secreted from infected cells was examined 24 h after infection and reported as ng/mL of GM-CSF per cell. n = 3 for biological replicates, ***, $p < 0.001$; ****, $p < 0.0001$; (n.s., no significance).

Next, we determined if virus-induced necrosis is immunogenic in nature. To accomplish this, we examined a panel of genes related to pro-inflammatory, anti-inflammatory, antigen presentation, and immune differentiation markers by qPCR. 24 h following infection with the viruses, we detected a general upregulation of genes related to immune cell recruitment and activation in MB49 cells. Notably, mouse *CCL5*, *CXCL10*, and *GM-CSF* transcripts showed an increase in expression in MB49 cells following VSVd51-mGM-CSF infection compared with VSVd51 and non-infected controls (Figure 2D). These data suggest enhanced immunogenic gene expression in MB49 cells following VSVd51-mGM-CSF-induced ICD.

Enhanced immune cell activation following VSVd51-mGM-CSF treatment in the syngeneic C57Bl/6-MB49 mouse model

To determine if the observed *in vitro* ICD and immune gene signatures in mouse BC cells translate to improved immune function *in vivo*, we compared VSVd51 and VSVd51-mGM-CSF in the treatment of C57Bl/6 mice bearing orthotopic MB49 tumors (Figure 3A). MB49 is one of the most-used murine BC cell lines and shares pivotal immunological and cell surface characteristics with aggressive human BC.[19,29] At early and late time points following intravesical VSVd51-mGM-CSF treatment, we observed significantly increased proportions of $CD69^+$ (early lymphocyte activation), $IFN\gamma^+$ (cytokine

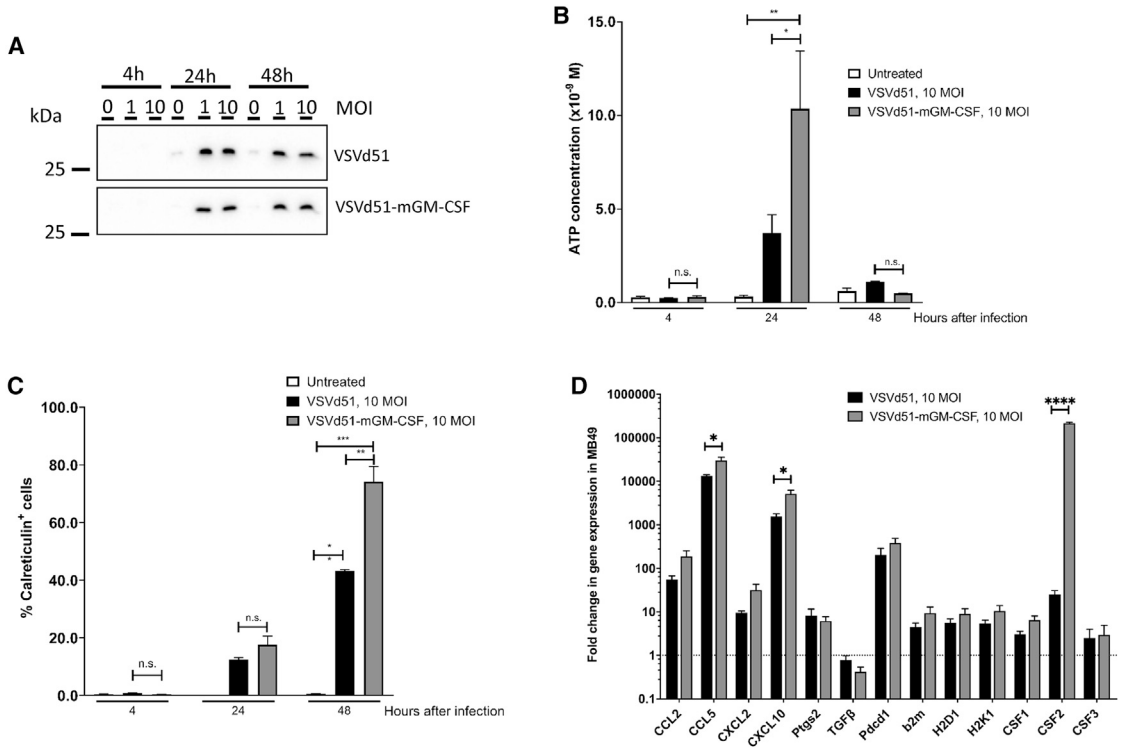

Figure 2. The GM-CSF transgene in VSVd51 induces enhanced immunogenic cell death and associated gene signature in the MB49 mouse bladder cancer cell line following infection

(A) Western blot analysis of HMGB1 from cell-free supernatants, (B) luminometry measurement of ATP from cell-free supernatants, and (C) measurement of cell surface calreticulin of the mouse MB49 BC cell line infected with VSVd51 and VSVd51-mGM-CSF at indicated MOI and following indicated time points. (D) Fold change in gene expression of MB49 cells following infection with VSVd51 and VSVd51-mGM-CSF at 10 MOI for 24 h. Quantitative PCR was performed using mRNA pooled from three independent experiments. All data are representative of at least three similar experiments where n = 3 for biological replicates, *, $p < 0.05$; **, $p < 0.01$; ***, $p < 0.001$; ****, $p < 0.0001$; (n.s., no significance).

production), and granzyme B^+ (cytotoxicity) peripheral blood NK cells compared with treatment with VSVd51 or PBS (Figure 3B). Similar results were observed with $CD11c^+$ cDC in terms of their activation status ($CD80^+/CD86^+$) (Figure 3C). Analysis of peripheral blood $CD3^+/CD8^+$ T cells showed increased IFNγ, and granzyme B in VSVd51-mGM-CSF-treated mice over controls (Figure 3D). However, the proportion of NK, DC, and $CD8^+$ T cell numbers in the periphery remained constant across treatments (Figures 3B–3D, first panel).

In contrast, both the proportion and function of bladder-infiltrating NK and $CD8^+$ T cells were significantly increased in VSVd51-mGM-CSF-treated mice (Figures 3E and 3F). In addition to immune effector cells, we assessed the proportion of regulatory cells, specifically in the tumor microenvironment (TME) of dissociated bladders. We did not observe any differences in T regulatory cell proportions across treatment groups (Figure 3G). However, we observed a significant decrease in granulocytic cells ($CD11b^+/Ly6G^{high}$) in VSVd51-treated groups compared with controls, while mice treated with VSVd51-mGM-CSF had reduced granulocytic cell proportions compared with PBS control, but had a higher proportion compared with VSVd51 (Figure 3H). In contrast, we did not observe any differences between VSVd51- and VSVd51-mGM-CSF-treated groups for monocytic cells other than a general decrease compared with PBS mice (Figure 3H). Lastly, we examined the functional suppressive capacity of granulocytic cell populations by examining arginase 1^+ ($ARG1^+$) and detected a greater proportion in VSVd51-mGM-CSF-treated mice compared with VSVd51 (Figure 3H). Taken together, these results suggest that while VSVd51 treatment diminished both myeloid regulatory cell population levels, treatment with VSVd51-mGM-CSF conversely enhanced the population of $ARG1^+$ granulocytic regulatory cells.

Increased T cell and myeloid cell populations detected by multiplex IF following VSVd51-mGM-CSF treatment in the syngeneic C57Bl/6-MB49 mouse model

Next, we wanted to determine the distribution of immune effector cell populations in the bladder tumor. Parallel to the flow cytometry experiments, bladders were harvested and stained for CD3, CD8, CD11b (myeloid cells), and CD208 (mature DC) with IF (Figure 4A). We were able to detect higher numbers of total $CD8^+$ and $CD11b^+$ cells in VSVd51-treated mice compared with controls (Figures 4C–

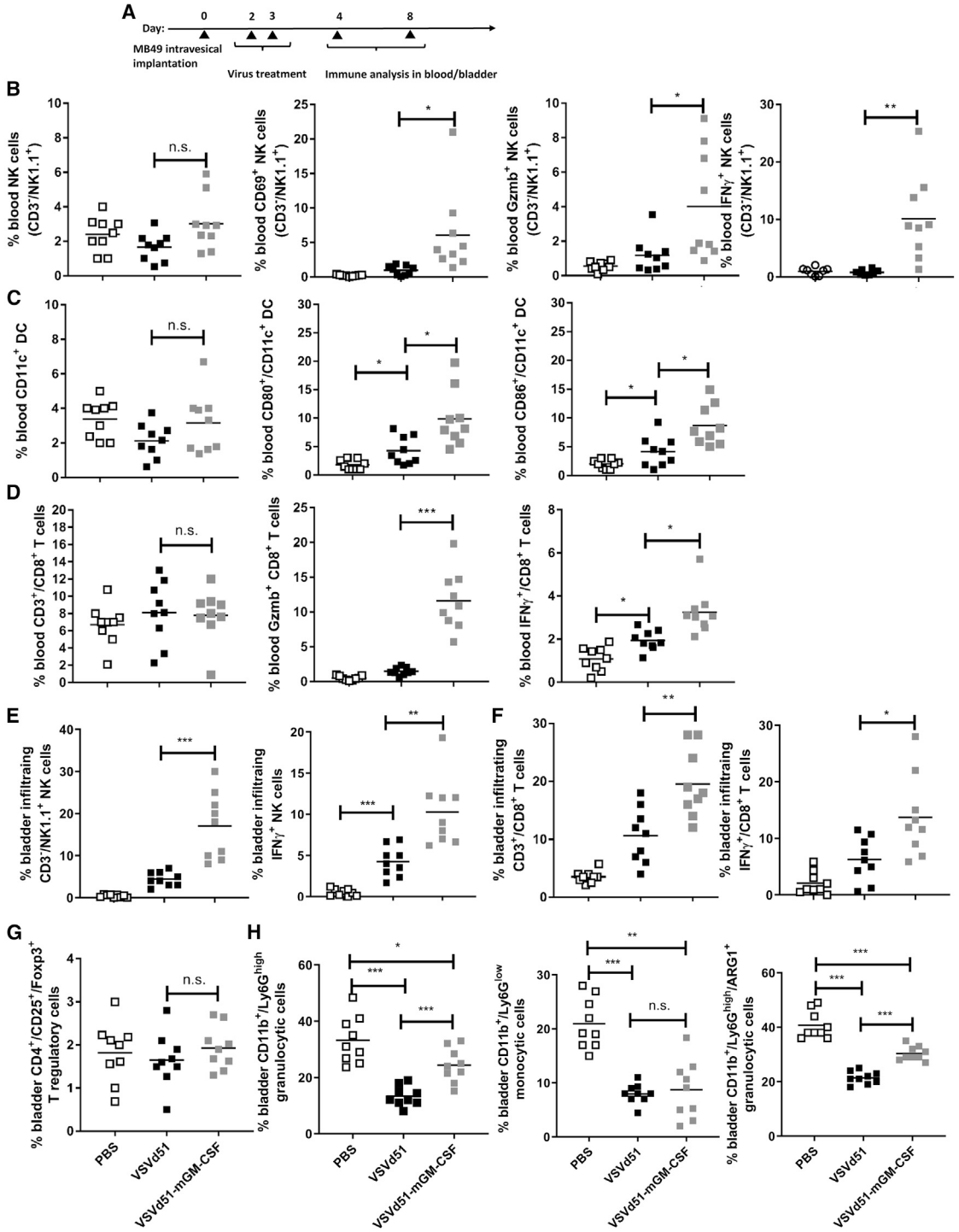

Figure 3. Enhanced immune cell activation following VSVd51-mGM-CSF treatment in the syngeneic C57Bl/6-MB49 mouse model

(A) Timeline of *in vivo* C57Bl/6-MB49 experiment. B6 mice bladders were instilled with 1×10^6 MB49 cells. Two days later, each group of mice received via intravesical instillation 50 μL of 5×10^8 PFU of VSVd51 or VSVd51-mGM-CSF or vehicle for control groups. Innate immune cells (B and C) were assessed via peripheral blood at day 4 post tumor implantation. Adaptive and regulatory immune cells (D–G) were assessed peripherally or in the bladder on day 8 post tumor implantation. Immune cell suspensions

(legend continued on next page)

4E). However, we detected significantly higher numbers of $CD3^+$, $CD8^+$, $CD8^+/CD3^+$, $CD11b^+$, and $CD208^+$ cells following VSVd51-mGM-CSF treatment compared with untreated mice (Figures 4B–4F). In particular, we observed higher levels of $CD3^+$, $CD8^+$, $CD8^+/CD3^+$, and $CD208^+$ cells in VSVd51-mGM-CSF-treated mice compared with VSVd51 treatment (Figures 4B–4D and 4F). Overall, these IF findings support our flow cytometry results and illustrate the potent immune-stimulating capacity of VSVd51-mGM-CSF as intravesical therapy for BC.

Diminished bladder tumor burden and improved survival in the C57Bl/6-MB49 model following VSVd51-mGM-CSF treatment is dependent on both immune effector and regulatory cells

To investigate whether the improved immune function of treated mice results in better disease outcome, we monitored mice for survival and measured tumor volume by small animal ultrasound. We observed reduced tumor volume and improved survival in VSVd51-mGM-CSF-treated mice compared with controls or VSVd51 (Figures 5A–5C). To confirm the critical role of NK and $CD8^+$ T cells after virus administration, we monitored for survival in VSVd51-mGM-CSF-treated mice that were pharmacologically depleted singly or of both immune cell populations (Figure 5D). In support of the *in vivo* data showing enhanced NK (Figure 3) and $CD8^+$ T cell function (Figures 3 and 4), the protective effect of treated mice with VSVd51-mGM-CSF was partially removed upon depletion of NK cells, but completely abrogated upon depletion of $CD8^+$ T cells or combination of NK and $CD8^+$ T cells (Figure 5E). These results suggest that the therapeutic benefit of VSVd51-mGM-CSF treatment is dependent upon both NK and $CD8^+$ T cells, but likely more dependent on $CD8^+$ T cells. To follow up on the granulocytic cell expansion and $ARG1^+$ results upon VSVd51-mGM-CSF administration, we questioned whether depletion of this suppressive myeloid cell subset could further improve survival. Following depletion with anti-Ly6G, we observed a modest, but significant improvement in survival in VSVd51-mGM-CSF-treated mice (Figure 5F). These *in vivo* results suggest that improved survival of mice following VSVd51-mGM-CSF treatment is positively associated with effector immune cells and negatively associated with myeloid regulatory cells.

Enhanced immunogenic cell death and activation of innate and adaptive immune cells following exposure of human BC spheroids to VSVd51-hGM-CSF

To test the translational potential of VSVd51-hGM-CSF, we examined its anti-cancer effect on human BC cell lines and primary human immune cells. We propagated the human 5637 and UM-UC-3 BC cell lines as 3D spheroids instead of 2D monolayers to better mimic the physiology of the bladder urothelium. Using these spheroids, we examined biomarkers of ICD including secreted HMGB1 and ATP following infection. In the cell-free supernatants of VSVd51-hGM-CSF-infected 5637 spheroids, we observed increased levels of HMGB1, while similar HMGB1 levels were observed in UM-UC-3 spheroids (Figure 6A). Increased ATP levels (Figure 6B) at both 24 and 48 h post-infection compared with VSVd51 and non-infected controls was detected in 5637 spheroids, while higher ATP levels in UM-UC-3 spheroids were detected at earlier time points (4 h, 16 h) due to the stability of the spheroid structures in culture. Similar to our mouse data, the presence of these DAMPs suggests a greater induction of ICD in human BC spheroids by VSVd51-hGM-CSF.

In co-culture experiments with $CD14^+$ human monocytes incubated with cell-free lysates from infected 5637 spheroids, we observed polarization of these monocytes toward an M1-like phenotype expressing higher levels of CD80, CD86, HLA-DR, and PD-L1, which has been previously suggested[30,31] to promote anti-tumor immune responses (Figure 6C). To examine the immune consequences of VSVd51-hGM-CSF infection on immune effector cells, we measured human NK and $CD8^+$ T cell migration. We observed increased migration of $CD3^-/CD56^+$ NK and $CD3^+/CD8^+$ T cells toward conditioned media (CM) of VSVd51-hGM-CSF-infected 5637 spheroids (Figure 6D). Taken together, these data using human cells demonstrate the immune-activating potential of VSVd51-hGM-CSF.

VSVd51-hGM-CSF enhances biomarkers of ICD and autologous immune cell activation in human BC patient-derived organoids

To test the clinical potential of VSVd51-hGM-CSF, we questioned whether it could elicit an immunogenic signature in human BC patient tissue. We, therefore, enrolled BC patients in the observational oVSV-bladder study (Ethics protocol #2018-2414). To better model the physiological structures of the bladder urothelium, we propagated these BC patient-derived tissues as 3D organoids *ex vivo* (Figures S2A and S2B). Organoids from patients 34 and 38 were infected with VSVd51 or VSVd51-hGM-CSF and ICD assays were conducted. HMGB1 release for both patients was detected at higher levels in VSVd51-hGM-CSF-infected organoids (Figure 7A), while ATP release was detected at higher levels in VSVd51-hGM-CSF-infected organoids for patient 34 (Figure 7B). Importantly, we looked at autologous immune cell activation following treatment of matched BC organoids with VSVd51-hGM-CSF (Figures 7C–7F). We observed enhanced CD107a degranulation in NK and $CD8^+$T cells following co-culture with autologous $CD11c^+$ DC incubated with CM from VSVd51-hGM-CSF-infected organoids compared with controls in both patients (Figures 7C and 7E). Additionally, we detected enhanced CD80, CD86, and HLA-DR expression on $CD11c^+$ autologous cDCs of patient 38 following incubation with CM from VSVd51-hGM-CSF-treated organoids compared with controls (Figure 7F). These human data demonstrate that an ICD signature is present in patient BC organoids following VSVd51-hGM-CSF infection, and

from the peripheral blood (B–D) or dissociated bladders (E–H) of mice following indicated treatments were stained with (B and E) NK cell markers ($NK1.1^+$, $CD3^-$, $CD69^+$, granzyme B^+, $IFN\gamma^+$), (C) DC markers ($CD11c^+$, $CD80^+$, $CD86^+$), (D and F) T cell markers ($CD3^+$, $CD8^+$, granzyme B^+, $IFN\gamma^+$), (G) T regulatory cells ($CD3^+$, $CD4^+$, $CD25^+$, $Foxp3^+$), (H) myeloid derived suppressor cells ($CD11b^+$, $Ly6G^+$, $ARG1^+$), and analyzed by flow cytometry. All data are representative of at least three similar experiments where n = 5–9 mice/treatment, *, $p < 0.05$; **, $p < 0.01$; ***, $p < 0.001$; (n.s., no significance).

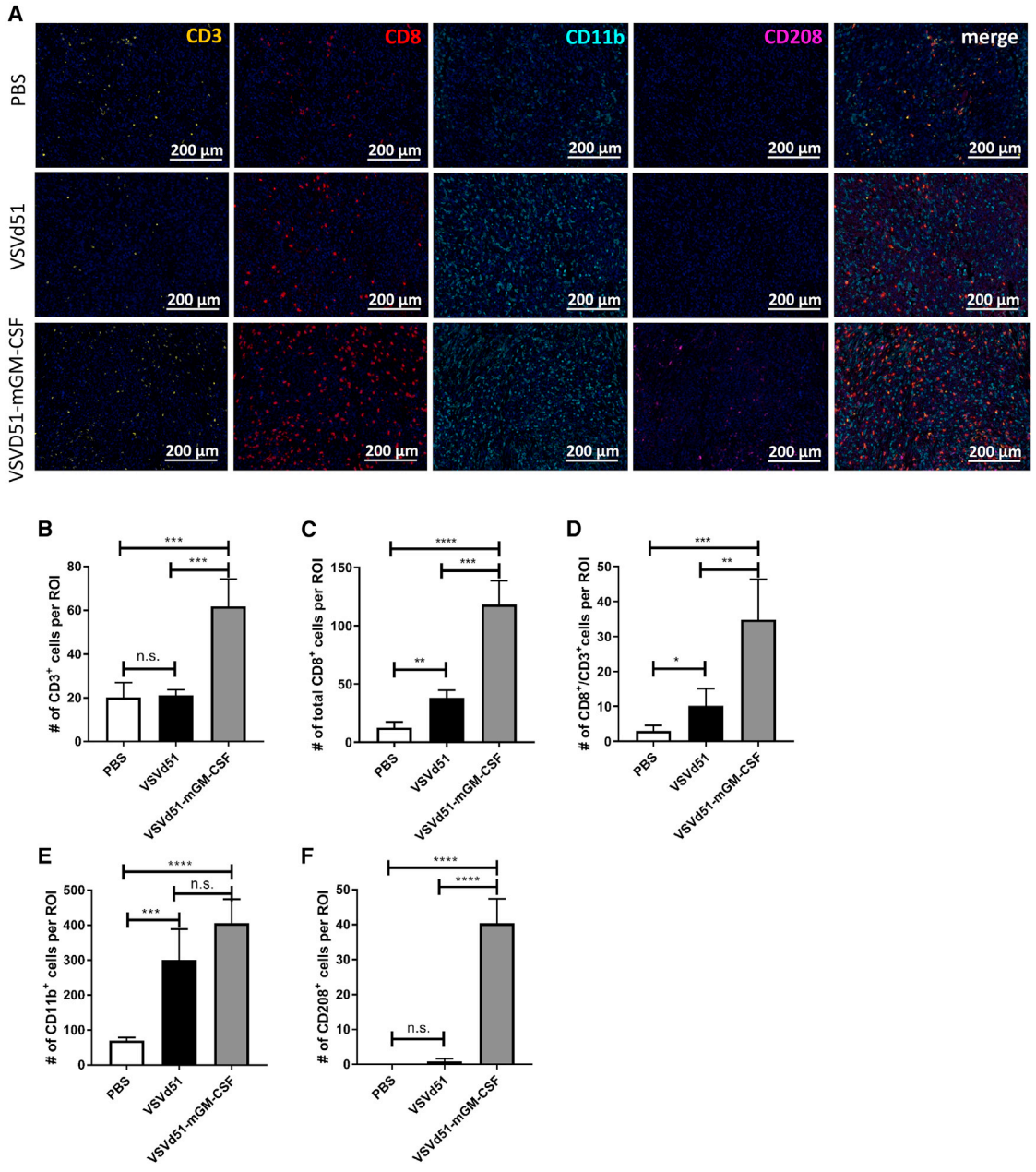

Figure 4. Increased T cell and myeloid cell populations detected by multiplex IF following VSVd51-mGM-CSF treatment in the syngeneic C57Bl/6-MB49 mouse model

Representative images (A) and quantification (B–F) of $CD3^+$, $CD8^+$, $CD8^+/CD3^+$, $CD11b^+$, and $CD208^+$ cells in PBS, VSVd51-, and VSVd51-mGM-CSF-treated mice. The percentage of positive cells was enumerated as averages from five to six regions of interest from three tissue slices each. Original magnification ×20. The scale bar is 200 µm. All data are representative of at least three similar experiments where n = 5–9 mice/treatment *, $p < 0.05$; **, $p < 0.01$; ***, $p < 0.001$; ****, $p < 0.0001$; (n.s., no significance).

this phenotype has the capacity to activate autologous immune cells *ex vivo*.

DISCUSSION

For patients who fail frontline therapies and who refuse or are not candidates for surgery, there is an urgent medical need for additional bladder-sparing treatments. The urinary bladder is an ideal organ to evaluate local virotherapy. First, the urethra permits easy intravesical instillation of OV providing cancer cells exposure to large viral titers. For safety considerations, the bladder is an isolated organ and the trilaminar unit membrane limits potential systemic viremia outside of the bladder walls. Finally, the success of

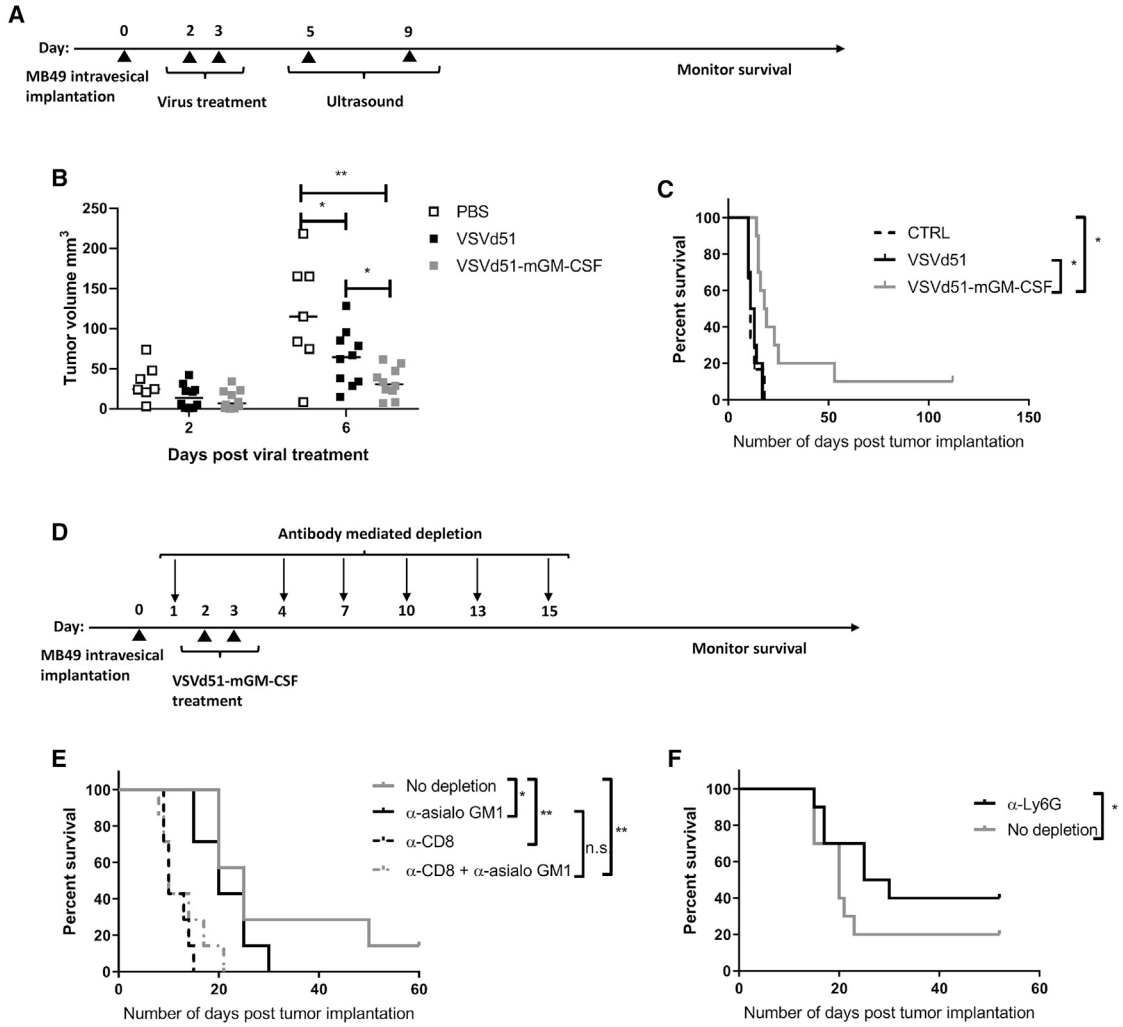

Figure 5. Diminished bladder tumor burden and improved survival in the C57Bl/6-MB49 model following VSVd51-mGM-CSF treatment is dependent on both immune effector and regulatory cells

(A) Timeline of *in vivo* C57Bl/6-MB49 experiment. B6 mice bladders were instilled with 1×10^6 MB49 cells. Two days later, each group of mice received via intravesical instillation 50 μL of 5×10^8 PFU of VSVd51 or VSVd51-mGM-CSF or vehicle for control groups. (B) Tumor volume assessment at days 2 and 6 following indicated treatments was performed via small animal ultrasound. (C) Kaplan-Meier survival analysis of C57Bl/6 mice bearing MB49 bladder tumors and treated with indicated therapies. (D) Timeline of immune cell depletion in the C57Bl/6-MB49 *in vivo* model. One day before virus treatment, NK cells, $CD8^+$ T cells, and NK + $CD8^+$ T cells were depleted using antibodies to GM1, CD8, GM1 + CD8, and Ly6G and continued every 3 days for a total of six doses. On days 2 and 3 following tumor implantation, all mice received VSVd51-mGM-CSF. (E and F) Kaplan-Meier survival analysis of C57Bl/6 mice bearing MB49 bladder tumors and receiving VSVd51-mGM-CSF and indicated antibody depletion or vehicle control. n = 10–12 mice/group. *, $p < 0.05$; **, $p < 0.01$; (n.s., no significance), log rank test.

BCG and adenovirus therapy for NMIBC demonstrates the sensitivity of BC to viro-immunotherapy.[24,29,32] Thus, in this report, we provide preclinical and translational immune response evidence for the use of oncolytic VSVd51-hGM-CSF for the treatment of BC.

From *in vitro* experiments, we determined that infection of mouse and human BC cells with VSVd51-mGM-CSF and VSVd51-hGM-CSF, respectively, results in higher ICD compared with VSVd51-infected and non-infected cells. We observed enhanced release of intracellular HMGB1 and ATP and increased $calreticulin^+/DAPI^+$ tumor cell populations (Figures 2 and 6). In these *in vitro* cultures, we postulate that the secreted GM-CSF is exerting an effect on cancer cells through known and unknown receptors and likely inducing endoplasmic reticulum stress and the unfolded protein response. The simultaneous virus infection and replication may dramatically increase cellular and oxidative stress, leading to increased bladder tumor cell death.[33,34] This novel role of virus-secreted GM-CSF in further amplifying ICD and its underlying mechanism is under investigation in our lab.

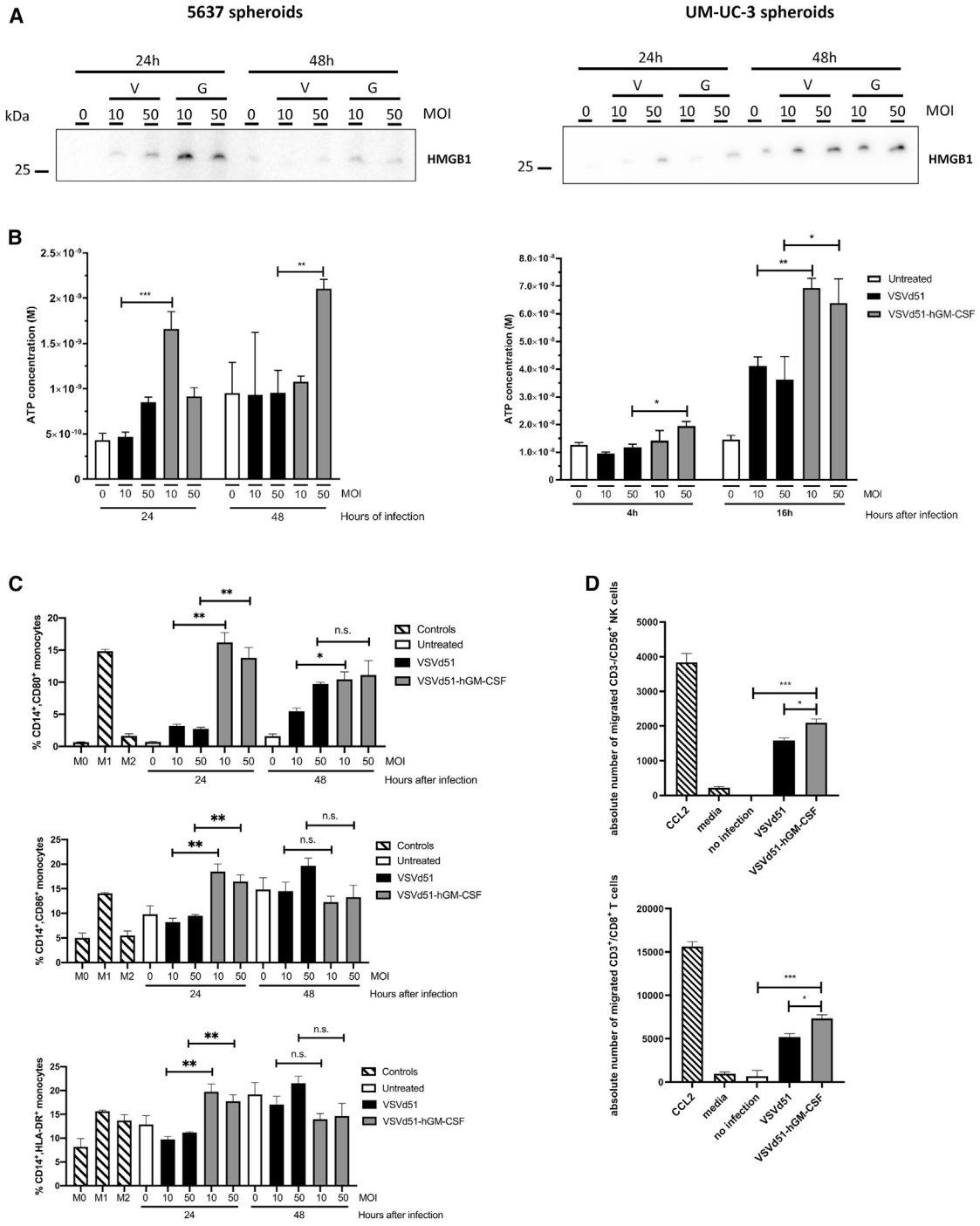

Figure 6. Enhanced immunogenic cell death and activation of innate and adaptive immune cells following exposure to VSVd51-hGM-CSF in human BC spheroids

(A) Western blot analysis of HMGB1 (V:VSVd51; G:VSVd51-hGM-CSF) and (B) luminometry measurement of ATP from cell-free supernatants of human BC 5637 and UM-UC-3 spheroids infected with VSVd51 and VSVd51-mGM-CSF at indicated MOI and following indicated time points. (C) Polarization of purified human monocytes in the presence of CM from human BC 5637 spheroids infected with VSVd51 or VSVd51-hGM-CSF at indicated MOI and time points. (D) Migration assay of human $CD3^{-}/CD56^{+}$ NK cells and $CD3^{+}/CD8^{+}$ T cells following exposure to CM from human BC 5637 spheroids infected with VSVd51 or VSVd51-hGM-CSF at indicated MOI and time points. CCL2 as positive control. All data are representative of at least three similar experiments where n = 3 for biological replicates. *, $p < 0.05$; **, $p < 0.01$; ***, $p < 0.001$; (n.s., no significance).

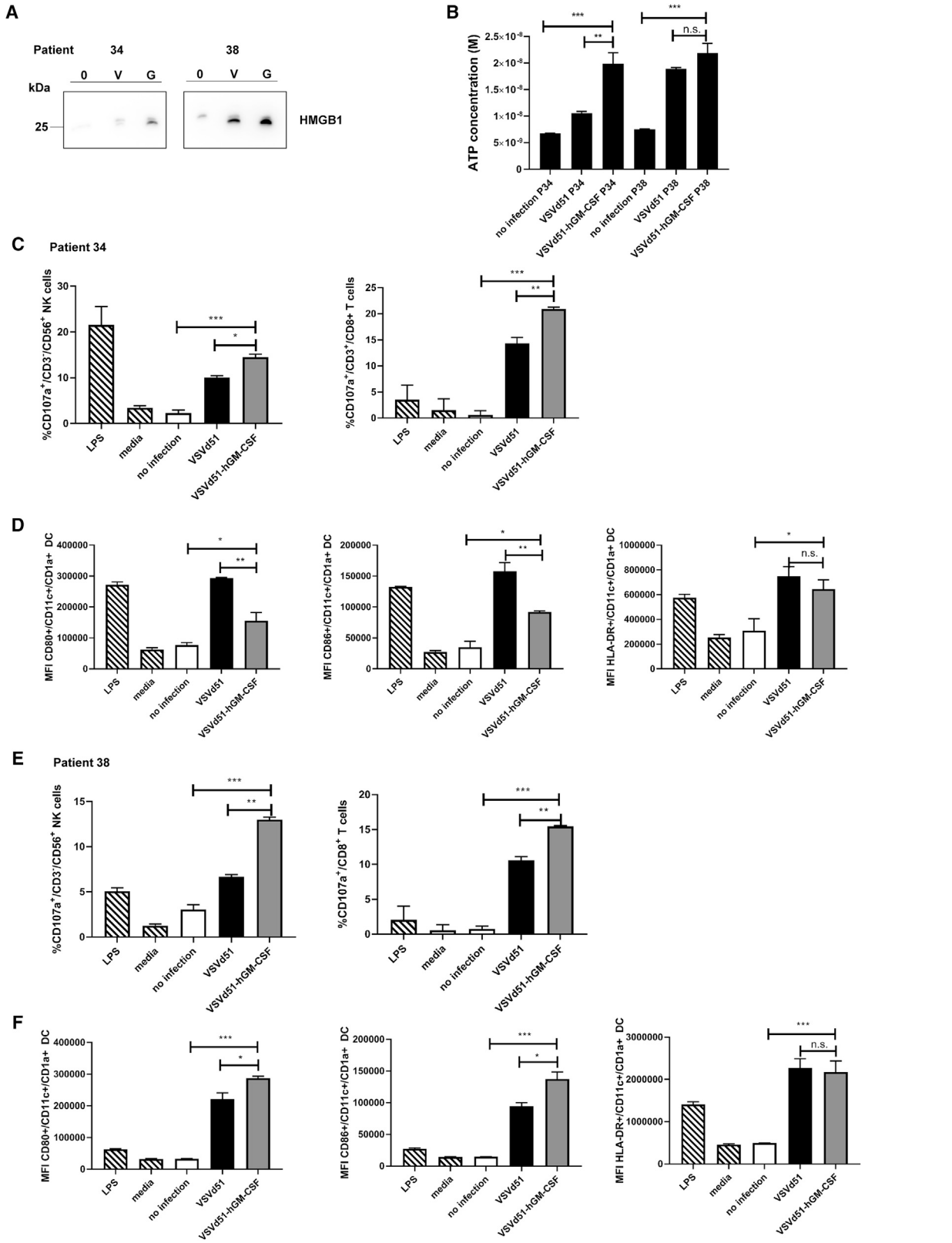

(legend on next page)

Previous studies have demonstrated that VSVd51 robustly recruits cDCs and activates effector NK cells to the site of tumor cell lysis through the release of HMGB1, exposure of calreticulin, and death receptor FasR-FasL expression.[35] In a separate report, VSVd51 increased the surface expression of MHC-I molecules in B16 melanoma cells following infection, which improved recognition by CD8+ T cells.[36] From our *in vivo* experiments, we observed that treatment of MB49 tumor-bearing mice with two doses of VSVd51-mGM-CSF significantly augmented both systemic and tumor-infiltrating innate and adaptive immune cell functionality, resulting in reduced bladder tumor burden and improved survival compared with treatment with parental VSVd51. Both NK and $CD8^+$ T cells were important in contributing toward VSVd51-mGM-CSF-mediated treatment efficacy as shown in depletion studies. However, $CD8^+$ T cells appear to play a more important role in mediating therapeutic efficacy as evidenced by shortened survival in $CD8^+$ T cell-depleted mice, singly or in combination with NK cells. While the overall survival in VSVd51-mGM-CSF-treated mice was improved, we observed accumulation of $ARG1^+$ granulocytic myeloid regulatory cells in the bladder tumor tissue of these mice (Figure 3H). These regulatory cells have been shown to expand in the tumor microenvironment and exert suppression on innate and adaptive immunity through production of regulatory enzymes.[37] While enhancing cDC proliferation and activation, GM-CSF may indiscriminately increase myeloid regulatory cell populations.[37–39] Therefore, the counter-regulatory activities of GM-CSF overexpression by VSVd51-mGM-CSF may be reducing its therapeutic efficacy by expanding granulocytic myeloid regulatory cells and subsequent inhibition of effector immune cells. Depletion studies with anti-Ly6G in the context of VSVd51-mGM-CSF treatment significantly improved survival in these cohorts (Figure 5F). While VSVd51-mGM-CSF significantly improves survival compared with VSVd51, we speculate that these regulatory cells, which resemble myeloid-derived suppressor cells, along with other regulatory mechanisms in the TME, may be contributing toward suboptimal VSVd51-mGM-CSF efficacy. The counter-regulatory activity of GM-CSF is an important limitation highlighted by our findings that could reduce the therapeutic efficacy of other OVs expressing GM-CSF, such as the FDA-approved oncolytic herpes simplex virus (HSV) for the treatment of end-stage melanoma.[40] Therefore, combination treatment with OV and immunomodulators to remove TME immune suppression may improve overall survival. These studies are underway in our lab.

In translational studies, we demonstrated that an analogous mechanism of VSVd51-hGM-CSF-induced immune activation is occurring in human BC spheroids and patient-derived organoids. VSVd51-hGM-CSF infection of human BC spheroids resulted in the enhanced release of immunogenic DAMPs and polarization of human monocytes toward an M1-like phenotype and lead to greater NK and $CD8^+$ T cell migration (Figure 6). In two BC patient-derived organoids (Figure S2A), evaluation of ICD biomarkers showed augmented release of DAMPs. The direct effect of GM-CSF on BC patient organoids in amplifying ICD is currently being explored in our lab. Importantly, autologous patient immune cells incubated with CM from VSVd51-hGM-CSF-infected matched organoids demonstrated enhanced innate and adaptive immune cell activation (Figure 7). Specifically, we observed increased activation of DCs via upregulation of costimulatory molecules CD80/CD86 in patient 38 along with an increase in CD107a degranulation marker on NK and $CD8^+$ T cells, which was also observed in patient 34. The DC are likely up-taking both viral and tumor-associated peptides in the supernatant of tumor cells infected by virus. The increased amounts of GM-CSF produced by VSVd51-hGM-CSF is enhancing the maturation/differentiating status of the DCs, which increases their capacity for viral/tumor antigen presentation to immune effector cells. Tumor-specific antigen responses in transgenic bladder tumor models in the context of virotherapy is a future focus of our lab.

Although only two patient BC tissues were tested, their permissiveness to VSVd51-hGM-CSF infection and resultant activation of autologous immune cells, despite patient 38 receiving systemic chemotherapy pre-surgery (Figures S2B and 7), justifies further testing of this novel virotherapy for BC. Previous studies have described the association between IFN responsiveness of bladder tumor cell lines and patient-derived tissues and sensitization to VSV-induced cell death.[11,12] Interestingly, higher-grade tumors (grades II and III) did not respond to IFN therapy, but responded well to VSV infection. Separate studies describe the expression of the low-density lipoprotein receptor (LDLR) in BC and its correlation with patient survival.[41] LDLR is the surface receptor used by VSV to gain entry into cells and appears to be highly expressed in high-grade tumors, BC included. These studies suggest the potential of selecting BC patients for VSV-based therapy based on IFNAR and/or LDLR expression on patient tissue. Taken together, these translational results demonstrate the feasibility of developing a VSVd51-hGM-CSF-based immunogenic virotherapy to treat BCG failed and high-risk patients.

MATERIALS AND METHODS

Cell lines and viruses

The murine BC cell line MB49 was maintained in DMEM; the human BC cell lines 5637 in RPMI and UM-UC-3 in EMEM, all supplemented with 10% HI FBS + 100 U/mL penicillin and 100 μg/mL streptomycin (complete media). 5637 and UM-UC-3 cell lines (both of male origin) were purchased from ATCC and MB49 cell line from Millipore-Sigma and were verified to be mycoplasma free and show appropriate microscopic morphology. All three BC cell

Figure 7. VSVd51-hGM-CSF enhances biomarkers of ICD and autologous immune cell activation in human BC patient-derived organoids

ICD and immune activation of BC patient-derived organoids from patients 34 and 38 as measured through (A) western blot analysis of HMGB1 (V:VSVd51; G:VSVd51-hGM-CSF); (B) luminometry measurement of ATP; (C–F) functionality of autologous human $CD8^+$ T and NK cells following co-culture with autologous treated-cDC and activation of autologous human cDCs in the presence of CM from infected human BC patient-derived organoids (patient 34 [C and D]; patient 38 [E and F]). All organoids were infected with VSVd51 or VSVd51-hGM-CSF at 10 MOI for 24 h. Data are pooled from biological replicates, n = 3, *, $p < 0.05$; **, $p < 0.01$; ***, $p < 0.001$; (n.s., no significance).

lines were chosen due to their invasive nature and their ability to assemble into 3D spheroid cultures. VSV-hGM-CSF was cloned from parental VSVd51. Briefly, polymerase chain amplification was used to amplify hGM-CSF from the pUNO1-hGM-CSF plasmid (Invivogen) and the cDNA was subcloned into VSVd51 via the restriction sites XhoI/NheI. This plasmid was used to rescue a recombinant VSVd51-hGM-CSF as previously described.[42] VSVd51 and VSVd51-mGM-CSF were obtained from the Ottawa Hospital Research Institute (Ottawa, Canada). All viruses were propagated on Vero cells and purified using Opti-Prep purification methods. Viral titers were determined by a standard plaque assay as previously published.[42] Viral cytotoxicity was assessed on the indicated cell lines, and cell viability using the non-radioactive MTT assay (Promega) was carried out as described previously.[42]

Mice

Female C57Bl/6 mice (6–8 weeks old, 20–25 g) were purchased from Charles River (Quebec). Animals were housed in pathogen-free conditions at the Central Animal Facility of the Université de Sherbrooke with access to food and water *ad libitum*. Animals were euthanized by cervical dislocation under anesthesia. All studies were conducted in accordance with university guidelines and the Canadian Council on Animal Care, and protocols were approved by the Faculty Animal Care Committee.

C57Bl/6-MB49 syngeneic mouse model of bladder cancer

For orthotopic implantation of BC cells, mice were anesthetized and chemical lesions were induced by intravesical instillation of trypsin (Wisent) 1:1 in DMEM. During this procedure, all mice were kept under anesthesia (3% induction, 1.5% maintenance of isoflurane with 2% O_2). Subsequently, 1×10^6 MB49 bladder tumor cells were instilled. Mice were randomized according to weights. Two days later, each group of mice received via intravesical instillation 50 µL of 5×10^8 PFU of VSVd51 or VSVd51-mGM-CSF or vehicle control. Screening of tumor-bearing mice prior to the initiation of virus treatment was conducted by ultrasound to ensure equal tumor burdens. For the *in vivo* depletion of immune cells, six doses of depletion antibodies (1 dose 24 h after tumor instillation, followed by five additional doses 3 days apart) were administered by intraperitoneal injection of 250 µg/dose for anti-mouse Ly6G (1A8; BioXCell); 20 µg/dose for anti-Asialo (GM1, Life Technologies), and 250 µg/dose for anti-CD8α (53-6.7, BioXCell). Bladder tumor growth was monitored biweekly by small animal ultrasound (Vevo3100, VisualSonics).

Mouse bladder tumor dissociation

Following euthanasia, bladders were immediately placed in cRPMI and processed using the mouse tumor dissociation kit (Miltenyi biotec). Briefly, bladders were cut into small pieces (<2 mm^3), then treated with dissociation enzymes and placed into the gentle MACS OctoDissociator (Mitenyi biotec). Following dissociation, macroscopic pieces were removed using a 70-µm nylon cell strainer. Single cell suspensions were washed twice in cRPMI and proceeded to flow cytometry acquisition as described below.

Flow cytometry

Antibodies are listed in Table S1. To analyze mouse blood and tumor dissociated lymphocyte populations, an initial incubation was done in ACK lysis buffer for 5 mins to lyse red blood cells. 1×10^6 cells were then added to each tube. Fc block was added prior to antibody staining for 10 min at room temperature. Samples were washed twice with flow cytometry buffer (PBS, 2% FBS, 1 mM EDTA) and acquired on a CytoFLEX 30 (Beckman Coulter). Data was analyzed with CytExpert software. For assessment of NK and T cell functionality, cells were cultured with PMA/ionomycin (Sigma) for 4 h in the presence of brefeldin A (1 µL/mL) at 37°C. After 4 h, cells were washed twice with PBS, and then stained for NK and T cell markers. Cells were then fixed and permeabilized using BD Cytofix/Cytoperm kit, according to the manufacturer's protocol, and intracellular staining for granzyme B and IFNγ was performed. The CD107a antibody was added to cells alongside PMA/ionomycin stimulation.

Multiplex immunofluorescence

FFPE tissue sections (4 µm) were processed manually. Briefly, slides were heated at 37°C overnight, deparaffinized, and then fixed in neutral-buffered 10% formalin. The presence of T cells (CD3), CD8 cells, myeloid cells (CD11b), or mature DC (CD208) were assessed using a serial same-species fluorescence-labeling approach that employs tyramide signal amplification and microwave-based antigen retrieval and antibody stripping in accordance with the manufacturer's instructions (Opal Multiplex IHC, PerkinElmer). Antibodies are listed in Table S1. Staining was visualized using the Vectra3 imaging system (Akoya Biosciences). Following whole slide scan, areas of interest on tissue sections were annotated using Phenochart for 20x multispectral images.

Immunogenic cell death assays

For monolayer cultures, CM was obtained by seeding 5×10^5 cells in 12-well plates in their corresponding media for 24 h followed by infection with VSVd51 and VSVd51-m/hGM-CSF at the indicated PFU for the indicated time points. For 5637 spheroids, CM was obtained by resuspending 2.5×10^4 5637 cells in 20 µL of Matrigel (Corning) per well of a 48-well (Thermo Fisher Scientific) plate for 6 days followed by infection with VSVd51 and VSVd51-hGM-CSF. Calreticulin, HMGB1 and ATP measurements were conducted as previously described.[43] Briefly, calreticulin exposure was measured by flow cytometry, and HMGB1 and ATP protein levels were measured by western blot and luminometry, respectively (Table S1 for all antibodies).

Quantitative PCR

Total RNA was extracted from fresh virus-infected or mock-infected cells or organoids using Trizol (Invitrogen) according to the manufacturer's protocol. Quantitative PCR was performed using RNA pooled from three independent experiments. RNA was then used for reverse transcription and qPCR, which was performed, validated, and analyzed by the RNomics Platform at the Université de Sherbrooke (Bio-Rad CFX RealTime system) according to the protocols previously established by Hellemans et al.[44] and

Vandesompele et al.[45] RNA integrity was assessed with an Agilent 2100 Bioanalyzer (Agilent Technologies). All forward and reverse primers are listed in Table S2.

ELISA

Culture supernatants were diluted 5-fold. ELISA kits (Peprotech) for detecting mouse and human GM-CSF were performed according to manufacturer's instructions.

Human immune cell polarization and migration assays

Monocyte polarization

Human monocytes were isolated from peripheral blood (Human $CD14^+$ isolation kit, STEMCELL). 5×10^5 monocytes were seeded in 24-well plates in complete RPMI and incubated overnight at 37°C and 5% CO_2. 24 h later, the monocyte media was replaced with the CM of infected human cell lines. Controls were used as previously published.[43] Antibodies are listed in Table S1.

Immune cell migration

200 µL of CM was placed in the lower well of Boyden chambers, separated from the top well by 5-µm-pore polycarbonate filters (Neuro Probe). 6×10^5 human PBMC was added to the top chamber, followed by incubation at 37°C, 5% CO_2 for 45 mins. Next, the media in the top of the chamber was aspirated and the membrane removed with forceps. This was followed by harvesting of media in the bottom chamber and quantification of migrated cells by flow cytometry for CD3, CD8, and CD56 extracellular markers. CCL2 was used as a positive control.

BC patient tumor dissociation

Bladder tumor tissue from patients 34 and 38 was collected after surgery (Human protocol #: 2018-2465, approved by the human ethics review board of the CIUSSS de l'Estrie CHUS) and placed in cDMEM. Tumors were dissociated using the human tumor dissociation kit with the gentle MACS OctoDissociator (Miltenyi biotec) as described for mouse bladder dissociation. Cells were viably frozen down or freshly used for downstream experiments.

Human bladder cancer organoids

Viably frozen or freshly dissociated cells (1×10^5) were collected by centrifugation and resuspended in 20 µL of Matrigel (Corning) and plated in a prewarmed 48-well plate. Following Matrigel solidification, human bladder organoid media was added (Adv. DMEM/F-12, 100 ng/mL FGF10, 25 ng/mL FGF7, 12.5 ng/mL FGF2 [Peprotech], 1x B27 supplement [ThermoFisher], 5 µM A83-01, 1.25 mM N-acetylcysteine, and 10 mM nicotinamide [sigma]). Human BC organoids were passaged biweekly by dissociation using TrypLE (ThermoFisher). 10 µM ROCK inhibitor (Y-27632) was added to the media after passaging to prevent cell death. Organoids were frozen in freezing media (90% FBS, 10% DMSO) and could be recovered efficiently. OV infection of organoids was performed as described for 5637 and UM-UC-3 spheroids in ICD assays.

Ex vivo human T, NK, and dendritic cell activation

Immature DCs were obtained by CD14 positive selection (STEMCELL) according to manufacturer's guidelines from frozen human PBMCs. Sorted cells were incubated for 6 days with 500 U/mL of recombinant human IL-4 and 50 ng/mL of recombinant human GM-CSF (Bio Basic). For DC:PBMC co-culture assays, matched PBMCs were thawed and incubated for 24 h with 100 U/mL of recombinant human IL-2 (Bio Basic). Then, DCs and lymphoid cells were incubated an additional 24 h with CM from infected autologous organoids and acquired by flow cytometry for CD80/86 and HLA-DR on $CD11c^+/CD1a^+$ cDCs. T and NK cell CD107a degranulation assessment was done by flow cytometry following co-culture with autologous DCs. Antibodies are listed in Table S1.

Statistical analysis

All analyses were conducted using Prism 7 (GraphPad). Unpaired two-tailed *t* tests were used for comparing cell cultures and mice experiments that included two treatment groups. To determine statistically significant differences between response levels among more than two treatment groups, we applied two-way ANOVA and Tukey's post-hoc tests. Survival studies were assessed using Kaplan-Meier curves and analyzed by log rank testing. $P < 0.05$ was considered statistically significant.

SUPPLEMENTAL INFORMATION

Supplemental information can be found online at https://doi.org/10.1016/j.omto.2022.01.009.

ACKNOWLEDGMENTS

The authors thank the patients who consented to participate in this study. The authors also thank all the institutional and federal funding support. CIHR New Investigator Award (L.T.) and FRQS Jr 1 Salary Awards (L.T., P.R.) provided salary support; Université de Sherbrooke Chair (CRMUS) in Translational Immunotherapy Research (L.T.) and CRCHUS Team Grant (L.T., P.R.) provided operating funds for this study; Université de Sherbrooke, Graduate Scholarship provided the student scholarship for C.R.

AUTHOR CONTRIBUTIONS

C.R., C.L., F.B-G., S.R.N., M.B., S.R., A.S., A-O.G-C., C.I., N.E.N., and M.K. executed experiments, acquired and analyzed data, read and approved the manuscript; C.R., C.L., C.I., M.K., P.R., and L.T. contributed to writing, revising and editing the manuscript; L.T. and P.R. acquired funding and supervised the study.

DECLARATION OF INTEREST

L.T. declares that a patent application covering the use of VSVd51-hGM-CSF for bladder cancer is pending.

REFERENCES

1. Richters, A., Aben, K.K.H., and Kiemeney, L. (2020). The global burden of urinary bladder cancer: an update. World J. Urol. *38*, 1895–1904.

2. Babjuk, M., Bohle, A., Burger, M., Capoun, O., Cohen, D., Comperat, E.M., Hernandez, V., Kaasinen, E., Palou, J., Roupret, M., et al. (2017). EAU guidelines

on non-muscle-invasive urothelial carcinoma of the bladder: update 2016. Eur. Urol. *71*, 447–461.

3. Society, C.C. (2016). Canadian Cancer Statistics 2016*vol 2017* (Statistics Canada).
4. Anastasiadis, A., and de Reijke, T.M. (2012). Best practice in the treatment of non-muscle invasive bladder cancer. Ther. Adv. Urol. *4*, 13–32.
5. Chang, S.S., Bochner, B.H., Chou, R., Dreicer, R., Kamat, A.M., Lerner, S.P., Lotan, Y., Meeks, J.J., Michalski, J.M., Morgan, T.M., et al. (2017). Treatment of nonmetastatic muscle-invasive bladder cancer: American Urological Association/American Society of Clinical Oncology/American Society for Radiation Oncology/Society of Urologic Oncology Clinical practice guideline summary. J. Oncol. Pract. *13*, 621–625.
6. Kamat, A.M., Bellmunt, J., Galsky, M.D., Konety, B.R., Lamm, D.L., Langham, D., Lee, C.T., Milowsky, M.I., O'Donnell, M.A., O'Donnell, P.H., et al. (2017). Society for immunotherapy of cancer consensus statement on immunotherapy for the treatment of bladder carcinoma. J. Immunother. Cancer *5*, 68.
7. Huguet, J., Crego, M., Sabate, S., Salvador, J., Palou, J., and Villavicencio, H. (2005). Cystectomy in patients with high risk superficial bladder tumors who fail intravesical BCG therapy: pre-cystectomy prostate involvement as a prognostic factor. Eur. Urol. *48*, 53–59, discussion 59.
8. Stein, J.P., Lieskovsky, G., Cote, R., Groshen, S., Feng, A.C., Boyd, S., Skinner, E., Bochner, B., Thangathurai, D., Mikhail, M., et al. (2001). Radical cystectomy in the treatment of invasive bladder cancer: long-term results in 1,054 patients. J. Clin. Oncol. *19*, 666–675.
9. Lightfoot, A.J., Rosevear, H.M., and O'Donnell, M.A. (2011). Recognition and treatment of BCG failure in bladder cancer. ScientificWorldJournal *11*, 602–613.
10. Joudi, F.N., Smith, B.J., and O'Donnell, M.A.; National BCG-Interferon Phase 2 Investigator Group (2006). Final results from a national multicenter phase II trial of combination bacillus Calmette-Guerin plus interferon alpha-2B for reducing recurrence of superficial bladder cancer. Urol. Oncol. *24*, 344–348.
11. Zhang, K.X., Matsui, Y., Hadaschik, B.A., Lee, C., Jia, W., Bell, J.C., Fazli, L., So, A.I., and Rennie, P.S. (2010). Down-regulation of type I interferon receptor sensitizes bladder cancer cells to vesicular stomatitis virus-induced cell death. Int. J. Cancer *127*, 830–838.
12. Hadaschik, B.A., Zhang, K., So, A.I., Fazli, L., Jia, W., Bell, J.C., Gleave, M.E., and Rennie, P.S. (2008). Oncolytic vesicular stomatitis viruses are potent agents for intravesical treatment of high-risk bladder cancer. Cancer Res. *68*, 4506–4510.
13. Stojdl, D.F., Lichty, B.D., tenOever, B.R., Paterson, J.M., Power, A.T., Knowles, S., Marius, R., Reynard, J., Poliquin, L., Atkins, H., et al. (2003). VSV strains with defects in their ability to shutdown innate immunity are potent systemic anti-cancer agents. Cancer Cell *4*, 263–275.
14. Miest, T.S., Yaiw, K.C., Frenzke, M., Lampe, J., Hudacek, A.W., Springfeld, C., von Messling, V., Ungerechts, G., and Cattaneo, R. (2011). Envelope-chimeric entry-targeted measles virus escapes neutralization and achieves oncolysis. Mol. Ther. *19*, 1813–1820.
15. Patterson, C.E., Lawrence, D.M., Echols, L.A., and Rall, G.F. (2002). Immune-mediated protection from measles virus-induced central nervous system disease is noncytolytic and gamma interferon dependent. J. Virol. *76*, 4497–4506.
16. Achard, C., Surendran, A., Wedge, M.E., Ungerechts, G., Bell, J., and Ilkow, C.S. (2018). Lighting a fire in the tumor microenvironment using oncolytic immunotherapy. EBioMedicine *31*, 17–24.
17. Niavarani, S.R., Lawson, C., and Tai, L.H. (2019). Treatment of metastatic disease through natural killer cell modulation by infected cell vaccines. Viruses *11*, 434.
18. Tai, L.H., de Souza, C.T., Belanger, S., Ly, L., Alkayyal, A.A., Zhang, J., Rintoul, J.L., Ananth, A.A., Lam, T., Breitbach, C.J., et al. (2013). Preventing postoperative metastatic disease by inhibiting surgery-induced dysfunction in natural killer cells. Cancer Res. *73*, 97–107.
19. Annels, N.E., Arif, M., Simpson, G.R., Denyer, M., Moller-Levet, C., Mansfield, D., Butler, R., Shafren, D., Au, G., Knowles, M., et al. (2018). Oncolytic immunotherapy for bladder cancer using coxsackie A21 virus. Mol. Ther. Oncolytics *9*, 1–12.
20. Park, B.H., Hwang, T., Liu, T.C., Sze, D.Y., Kim, J.S., Kwon, H.C., Oh, S.Y., Han, S.Y., Yoon, J.H., Hong, S.H., et al. (2008). Use of a targeted oncolytic poxvirus, JX-594, in patients with refractory primary or metastatic liver cancer: a phase I trial. Lancet Oncol. *9*, 533–542.
21. Derubertis, B.G., Stiles, B.M., Bhargava, A., Gusani, N.J., Hezel, M., D'Angelica, M., and Fong, Y. (2007). Cytokine-secreting herpes viral mutants effectively treat tumor in a murine metastatic colorectal liver model by oncolytic and T-cell-dependent mechanisms. Cancer Gene Ther. *14*, 590–597.
22. Ramesh, N., Ge, Y., Ennist, D.L., Zhu, M., Mina, M., Ganesh, S., Reddy, P.S., and Yu, D.C. (2006). CG0070, a conditionally replicating granulocyte macrophage colony-stimulating factor–armed oncolytic adenovirus for the treatment of bladder cancer. Clin. Cancer Res. *12*, 305–313.
23. Harzstark, A.L., and Small, E.J. (2009). Immunotherapeutics in development for prostate cancer. Oncologist *14*, 391–398.
24. Boorjian, S.A., Alemozaffar, M., Konety, B.R., Shore, N.D., Gomella, L.G., Kamat, A.M., Bivalacqua, T.J., Montgomery, J.S., Lerner, S.P., Busby, J.E., et al. (2021). Intravesical nadofaragene firadenovec gene therapy for BCG-unresponsive non-muscle-invasive bladder cancer: a single-arm, open-label, repeat-dose clinical trial. Lancet Oncol. *22*, 107–117.
25. Lemay, C.G., Rintoul, J.L., Kus, A., Paterson, J.M., Garcia, V., Falls, T.J., Ferreira, L., Bridle, B.W., Conrad, D.P., Tang, V.A., et al. (2012). Harnessing oncolytic virus-mediated antitumor immunity in an infected cell vaccine. Mol. Ther. *20*, 1791–1799.
26. Ramsburg, E., Publicover, J., Buonocore, L., Poholek, A., Robek, M., Palin, A., and Rose, J.K. (2005). A vesicular stomatitis virus recombinant expressing granulocyte-macrophage colony-stimulating factor induces enhanced T-cell responses and is highly attenuated for replication in animals. J. Virol. *79*, 15043–15053.
27. Garg, A.D., Galluzzi, L., Apetoh, L., Baert, T., Birge, R.B., Bravo-San Pedro, J.M., Breckpot, K., Brough, D., Chaurio, R., Cirone, M., et al. (2015). Molecular and translational classifications of DAMPs in immunogenic cell death. Front. Immunol. *6*, 588.
28. Pitt, J.M., Kroemer, G., and Zitvogel, L. (2017). Immunogenic and non-immunogenic cell death in the tumor microenvironment. Adv. Exp. Med. Biol. *1036*, 65–79.
29. Potts, K.G., Hitt, M.M., and Moore, R.B. (2012). Oncolytic viruses in the treatment of bladder cancer. Adv. Urol. *2012*, 404581.
30. Erdag, G., Schaefer, J.T., Smolkin, M.E., Deacon, D.H., Shea, S.M., Dengel, L.T., Patterson, J.W., and Slingluff, C.L., Jr. (2012). Immunotype and immunohistologic characteristics of tumor-infiltrating immune cells are associated with clinical outcome in metastatic melanoma. Cancer Res. *72*, 1070–1080.
31. Iannello, A., Thompson, T.W., Ardolino, M., Marcus, A., and Raulet, D.H. (2016). Immunosurveillance and immunotherapy of tumors by innate immune cells. Curr. Opin. Immunol. *38*, 52–58.
32. So, A., Rennie, P.S., and Jia, W. (2012). Intravesical oncoviral therapy for bladder cancer. J. Urol. *188*, 2039–2040.
33. Subramanian, M., Thorp, E., and Tabas, I. (2015). Identification of a non-growth factor role for GM-CSF in advanced atherosclerosis: promotion of macrophage apoptosis and plaque necrosis through IL-23 signaling. Circ. Res. *116*, e13–e24.
34. Hong, I.S. (2016). Stimulatory versus suppressive effects of GM-CSF on tumor progression in multiple cancer types. Exp. Mol. Med. *48*, e242.
35. Simovic, B., Walsh, S.R., and Wan, Y. (2015). Mechanistic insights into the oncolytic activity of vesicular stomatitis virus in cancer immunotherapy. Oncolytic Virother. *4*, 157–167.
36. Janelle, V., Langlois, M.P., Lapierre, P., Charpentier, T., Poliquin, L., and Lamarre, A. (2014). The strength of the T cell response against a surrogate tumor antigen induced by oncolytic VSV therapy does not correlate with tumor control. Mol. Ther. *22*, 1198–1210.
37. Umansky, V., and Sevko, A. (2013). Tumor microenvironment and myeloid-derived suppressor cells. Cancer Microenviron. *6*, 169–177.
38. Ostrand-Rosenberg, S. (2010). Myeloid-derived suppressor cells: more mechanisms for inhibiting antitumor immunity. Cancer Immunol. Immunother. *59*, 1593–1600.
39. Serafini, P., Carbley, R., Noonan, K.A., Tan, G., Bronte, V., and Borrello, I. (2004). High-dose granulocyte-macrophage colony-stimulating factor-producing vaccines impair the immune response through the recruitment of myeloid suppressor cells. Cancer Res. *64*, 6337–6343.
40. Rehman, H., Silk, A.W., Kane, M.P., and Kaufman, H.L. (2016). Into the clinic: talimogene laherparepvec (T-VEC), a first-in-class intratumoral oncolytic viral therapy. J. Immunother. Cancer *4*, 53.

41. Gonias, S.L., Karimi-Mostowfi, N., Murray, S.S., Mantuano, E., and Gilder, A.S. (2017). Expression of LDL receptor-related proteins (LRPs) in common solid malignancies correlates with patient survival. PLoS One *12*, e0186649.

42. Alkayyal, A.A., Tai, L.H., Kennedy, M.A., de Souza, C.T., Zhang, J., Lefebvre, C., Sahi, S., Ananth, A.A., Mahmoud, A.B., Makrigiannis, A.P., et al. (2017). NK-cell recruitment is necessary for eradication of peritoneal carcinomatosis with an IL12-expressing Maraba virus cellular vaccine. Cancer Immunol. Res. *5*, 211–221.

43. Niavarani, S.R., Lawson, C., Boudaud, M., Simard, C., and Tai, L.H. (2020). Oncolytic vesicular stomatitis virus-based cellular vaccine improves triple-negative breast cancer outcome by enhancing natural killer and CD8(+) T-cell functionality. J. Immunother. Cancer *8*, e000465.

44. Hellemans, J., Mortier, G., De Paepe, A., Speleman, F., and Vandesompele, J. (2007). qBase relative quantification framework and software for management and automated analysis of real-time quantitative PCR data. Genome Biol. *8*, R19.

45. Vandesompele, J., De Preter, K., Pattyn, F., Poppe, B., Van Roy, N., De Paepe, A., and Speleman, F. (2002). Accurate normalization of real-time quantitative RT-PCR data by geometric averaging of multiple internal control genes. Genome Biol. *3*, 1–12.